Published in Materials Chemistry and Physics 91: 185-191, 2005

Full potential calculation of structural, electronic and optical properties of $KMgF_3$

M. Sahnoun[a,*], M. Zbiri[a], C. Daul[a], R. Khenata[b], H. Baltache[b], M. Driz[b]

[a] *Chemistry Department, University of Fribourg, Chemin du Musée 09, Fribourg CH-1700, Switzerland*
[b] *Laboratoire de Physique Quantique et de Modélisation Mathématique (LPQ3M), Département de Technologie, Université de Mascara, Mascara DZ-29000, Algeria*

Received 14 April 2004; received in revised form 8 November 2004; accepted 15 November 2004

Abstract

A theoretical study of the structural, electronic and optical properties of $KMgF_3$ is presented using the full-potential linearized augmented plane wave method (FP-LAPW). In this approach, the local density approximation was used for the exchange-correlation potentials. First, we present the main features of the structural and electronic properties of this compound, where the electronic band structure shows that the fundamental energy gap is indirect. The contribution of the different bands was analysed from the total and partial density of states curves. The different interband transitions have been determined from the imaginary part of the dielectric function. The results are compared with previous calculations and with experimental measurements. The present work also deals with the behaviour of electronic properties, namely, the energy band gaps, and the valence bandwidth of $KMgF_3$ subject of hydrostatic pressures up to 30 GPa.

PACS: 71.15.Mb; 71.15.Ap; 73.20.At; 74.25.Gz; 62.20.Dc

Keywords: Elasticity; Electronic band structure; Optical properties

1. Introduction

Technological demands on optical lithography in semiconductors require increasingly minute detail, and this in turn requires shorter wavelength lithographic light [1]. Hence vacuum-ultraviolet-transparent (VUV-transparent) materials for lenses in optical lithography steppers are desired. Perovskite structures, in general, are interesting materials for dielectric studies and several of them find application in optical, electronic and other solid-state devices. The ternary compounds belonging to the group of fluoroperovskites, having the general formula ABF_3, where A and B stands for alkali metals and alkaline earth metals, respectively, have recently received some attention in view of their possible use as lens materials because they do not have birefringence which makes design of lenses difficult [2–8]. Also, the possible problems in using optical materials for the UV and VUV regions are their limited transmission and the difficulty of material processing and polishing due to cleavage or the hydroscopic nature of the materials. $KMgF_3$ does not have these problems and, therefore, will be a suitable optical material for the UV and VUV regions, thus becoming more important for the next-generation of the lithographic technology [9]. Massa and Babel [10] have provided information on the equilibrium properties of this material, including lattice parameter, bulk moduli and lattice energy. Darabont et al. [11] investigated the $KMgF_3$ single crystals by X-ray diffraction and suggest that these crystals have a cubic perovskite structure with one molecule per unit cell, with lattice parameter $a = 3.978 \pm 0.05$ Å. Its structure is scheduled stable by many criteria [15,16] and, in fact, no phase transition has been observed for this compound. The elastic constants of this material were reported by Reshchikova [17] and Rosenberg

* Corresponding author. Tel.: +41 26 300 8749; fax: +41 26 300 9738.
E-mail address: mohammed.sahnoun@unifr.ch (M. Sahnoun).

0254-0584
doi:10.1016/j.matchemphys.2004.11.019

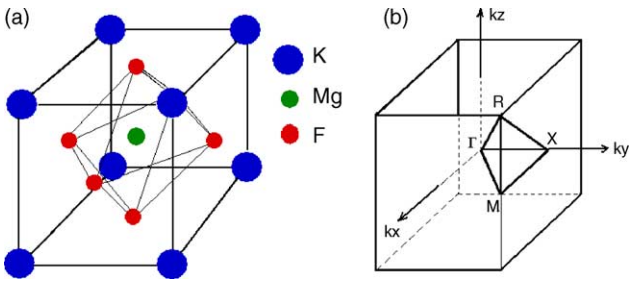

Fig. 1. (a) Crystal structure of $KMgF_3$. (b) Brillouin zone for the simple cubic lattice.

and Wigmore [18]; and the dielectric characteristics were also studied [19–21]. However detailed characteristics of $KMgF_3$ have not yet been well investigated. Our intention in this paper is to obtain a further understanding of structural, electronic and optical properties for this material by using full-potential linearized augmented-plane-wave calculations (FP-LAPW).

2. Computational details

The primitive cell for the ideal perovskite structure ABC_3 is illustrated in Fig. 1(a). For the perovskite-like fluoride $KMgF_3$, the body-center position is occupied by the alkali metal Mg atom, the edges by alkaline atoms K and the face centers by F atoms. The space group is $Pm\bar{3}m$ and the corresponding irreductible wedge in reciprocal space is shown in Fig. 1(b). The equilibrium structure, elastic constants and other properties of $KMgF_3$ were determined within the local density approximation (LDA) [22] as implemented in the wien2k package [23–25], using the full-potential linearized augmented-plane-wave method (FP-LAPW). The lattice is divided into muffin-tin spheres and an interstitial region. The muffin-tin radii used are 2.8, 1.65 and 1.65 a.u. for K, Mg and F, respectively. Inside the muffin-tin spheres, the wave functions charge densities, and potential are expanded in terms of the spherical harmonics. The cut-off angular momentum (L_{max}) is 10 for the wave functions. The Brillouin-zone integration is carried out using the improved tetrahedron method [26]. The number of the augmented plane waves included is about 533 per atom, i.e. $R_{MT}k_{max} = 7$. A $16 \times 16 \times 16$ grid of k-points is sampled in Brillouin zone to determine the self-consistent charge densities. The self-consistent cycles are terminated when the total energy cycles converges to within 0.1 mRy atom^{-1}.

3. Results and discussions

3.1. Total energy and elastic constants

The calculated total energy as a function of volume per atom for perovskite $KMgF_3$ is displayed in Fig. 2. The elastic moduli for an ideal perovskite structure may be divided into two parts, the bulk modulus $B = (C_{11} + 2C_{12})/3$, and the two shear moduli, C_{11}–C_{12} and C_{44}. The bulk modulus B is related to the curvature of $E(V)$, by a set of energies $E(V_i)$ for a discrete number of volumes V_i, and by making a least squares fit of the computed energies to the algebraic form proposed by Murnaghan [27], where we extract equilibrium volume V_0 of the unit cell, the equilibrium energy E_0 per unit cell at volume V_0, as well as the pressure derivative of the bulk modulus B'.

The shear moduli require knowledge of the derivative of the energy as a function of lattice strain [28] with preserved volume. Thus for the calculation of the modulus C_{11}–C_{12},

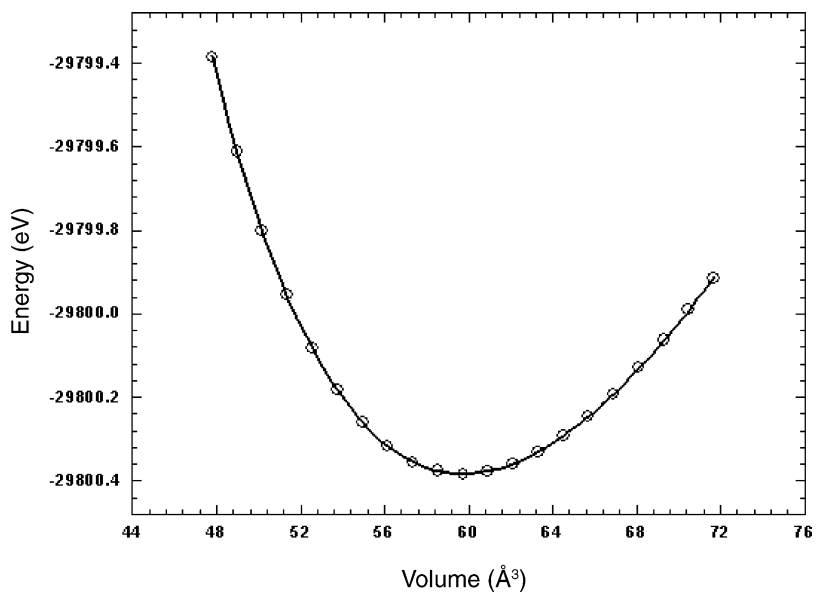

Fig. 2. Calculated total energy vs. relative volume in the perovskite $KMgF_3$.

Table 1
Calculated lattice constant (a_0), bulk modulus (B_0), pressure derivative of bulk modulus B', and elastic constants of $KMgF_3$

	a_0 (Å)	B (GPa)	B'	C_{11} (GPa)	C_{12} (GPa)	C_{44} (GPa)
Present	3.91	90.97	4.64	119.26	38.26	63.23
Exp.	3.978 ± 0.05[a], 3.973[b]	–	–	132[c]	39.6[c]	48.5[c]

The experimental values are also listed for comparison.
[a] Ref. [11].
[b] Ref. [13].
[c] Ref. [18].

we used the volume-conserving tetragonal strain tensor.

$$\vec{\varepsilon} = \begin{pmatrix} -\delta/2 & 0 & 0 \\ 0 & -\delta/2 & 0 \\ 0 & 0 & \delta \end{pmatrix} \quad (1)$$

Application of this strain changes the total energy from its unstrained value to

$$E(\delta) = E(-\delta) = E(0) + \tfrac{1}{2}(C_{11}-C_{12})V\delta^2 + \mathrm{O}[\delta^4] \quad (2)$$

where V is the volume of the unit cell and $E(0)$ the energy of the unrestrained lattice at volume V.

For the elastic modulus C_{44}, we used the volume-conserving trigonal strain tensor

$$\vec{\varepsilon} = \begin{pmatrix} 0 & \delta/2 & \delta/2 \\ \delta/2 & 0 & \delta/2 \\ \delta/2 & \delta/2 & 0 \end{pmatrix} \quad (3)$$

which changes the total energy to

$$E(\delta) = E(-\delta) = E(0) + \tfrac{3}{2}C_{44}V\delta^2 + \mathrm{O}[\delta^4] \quad (4)$$

Table 1 lists the calculated lattice parameter (a), bulk modulus (B) and its derivative (B') and elastic constants. As we can see, the lattice parameter is in excellent agreement with the experimental value. The calculated elastic constants compare very well with available experimental values.

3.2. Band structure and density of states

The first Brillouin zone is shown in Fig. 1(b), where symmetry points Γ(0, 0, 0), X(1, 0, 0), M(1, 1, 0) and R(1, 1, 1) are indicated in units of π/a along with the symmetry axes: $\Delta(x, 0, 0)$, $Z(1, x, 0)$, $\sum(x, x, 0)$, $T(1, 1, x)$, $\Lambda(x, x, x)$ and $S(1, x, x)$, x being in the range $0 < x < 1$. The calculated energy bands along the high-symmetry lines in the Brillouin zone for $KMgF_3$ are shown in Fig. 3. The width of the F 2p band (4.25 eV) and the energy difference between the K 3p and F 2p bands (7–8 eV) are in good agreement with experimental photoelectron spectroscopy data [32,33]. This band structure is representative of wide-gap-perovskite-like fluorides with indirect band gaps [29–31,34]; $KMgF_3$ has its conduction band minimum (CBM) at the Γ point and its valence band maximum (VBM) at the R point. The band gap width E_g is 7.8 eV which is much smaller than the experimental value of 12.4 eV [33,35,36]. The origin of this discrepancy is probably due to the use of LDA which generally underestimates the band gap in semiconductors and insulators [37]. The nine valence bands between −4.0 eV and the Fermi level (zero) are mainly due to p orbitals of F atoms. These nine valence bands are split into three triply degenerate levels at the Γ point (Γ_{15}, Γ_{25} and Γ_{15}) separated by energies of 0.25 eV (Γ_{15}–Γ_{25}) and 1.4 eV (Γ_{25}–Γ_{15}), due to the crystal field and electrostatic interaction between mainly three F atoms in the unit cell. The topmost valence bands are the F $2p_{x,y}$ states. In the conduction band region, the bottom is at Γ_1 state which is composed of s orbitals of all three kinds of atoms. The triply degenerate (Γ_{25}) and doubly degenerate (Γ_{12}) levels represent K 3d(t2g) and K 3d(eg) orbitals separated by energy of 2.2 eV. The first ones are from about 10 to 13 eV above the Fermi level arising from predominantly K 3d(t2g) states with a small F 2p mixing. The next bands belong to K 3d(eg) states. To further elucidate the nature of the electronic band structure, we have also calculated the total and atomic site projected densities of states (DOS) of $KMgF_3$. These are displayed in Fig. 4. The bands with the lowest energy, lying between −20 and −18.8 eV, correspond to a very large extend to F 2s states. The band around −8.8 eV is due to K 3p states. There is no mixing between s and p orbitals of the F atoms though allowed by symmetry. A large part of the bands connected to Γ_{12} and $\Gamma_{25'}$ is quite flat along the X–M direction. These bands correspond to Rydberg states with dominant K 3d character, such states correspond to conduction bands which have extreme sensitivity to external influences such as fields and in which one of the electrons has been excited. They range from 10 to 14.4 eV above the Fermi level.

3.3. Dielectric characteristics

The optical properties of matter can be described by the complex dielectric function $\varepsilon(\omega)$, which represents the linear response of a system due to an external electromagnetic field with a small wave vector. It can be expressed as [38–41]:

$$\varepsilon(\omega) = \varepsilon_1(\omega) + i\varepsilon_2(\omega) \quad (5)$$

where ε_1 and ε_2 are the real and imaginary components of the dielectric function, respectively. Calculations ignore excitonic effects but include the local-field effect. The direct interband contribution to the imaginary part of the dielectric function is calculated by taking all possible transitions

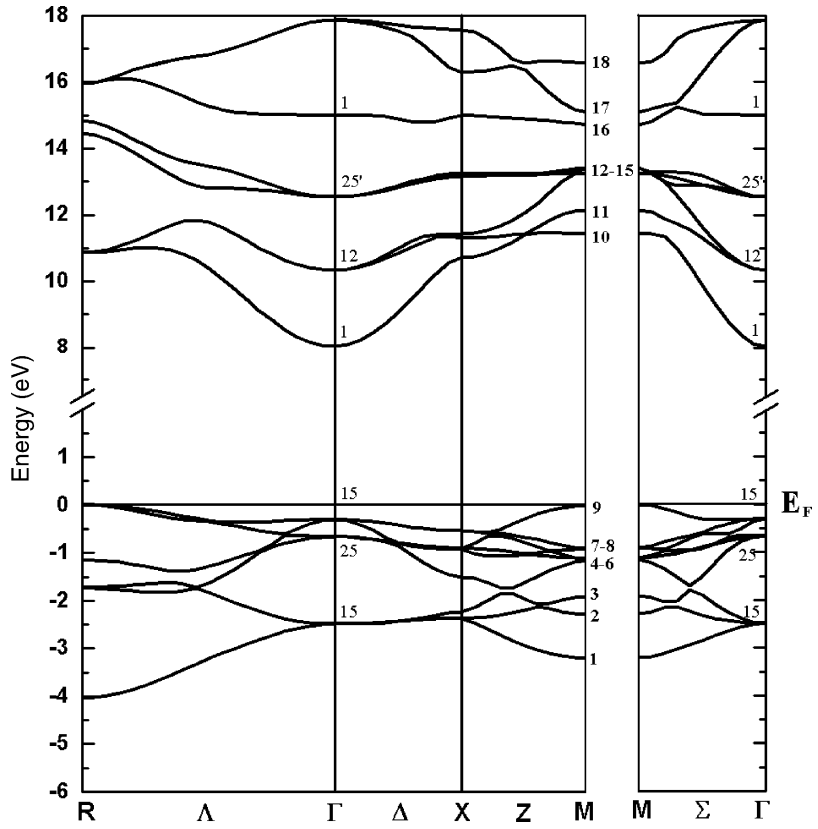

Fig. 3. Valence and conduction bands of $KMgF_3$ along some high-symmetry directions calculated using FP-LAPW method, within the LDA. The horizontal line shows the top of the valence band. The bands are numbered from the upper-valence band.

from occupied to unoccupied states, taking the appropriate transition matrix element into account [42,45].

$$\varepsilon_2(\omega) = \left(\frac{4\pi^2 e^2}{m^2\omega^2}\right) \sum_{ij} \int \langle i|M|j\rangle^2 f_i(1-f_i) \times \delta(E_f - E_i - \omega)\, \mathrm{d}^3k, \quad (6)$$

where M is the dipole matrix, i and j the initial and final states, respectively, f_i the Fermi distribution function for the ith state, and E_i the energy of electron in the ith state.

To give an overview of the optical properties of $KMgF_3$ and in particular to show the different optical interband transitions, the calculated dielectric function is shown in Fig. 5, including a life-time broadening of 0.15 eV in order to reduce the number of interband contributions to the essential ones.

Through the calculated electronic band structures and density of states, we can explain the different peak structures seen in Fig. 5. The origin of the peaks is investigated by decomposing $\varepsilon_2(\omega)$ into its partial band-to-band contributions, where the energy band surfaces in k-space are numbered in order of increasing energy irrespective of crossings along symmetry lines. This type of decomposition leads to the general assignments of peaks mentioned above. Regions of low dispersion in the interband transition energy surface indicate nearly parallel bands and hence large joint densities of states.

In this way, the spectra can be divided into four main peaks; the first peak at 11.53 eV is mainly due to the transitions from the last valence band to the second conduction band, from a region RΓM plane, where the bands are parallel. The second peak at 13.11 eV is due to transitions from bands 7 and 8 to band 13 in the ΓX direction near Γ. There is also significant contribution from band 9 to band 14 in the RΓ direction near Γ, and from band 3 to band 11 in the direction of RΓ direction and at X point. The third peak at 14.97 eV originate from transitions from the first valence band to band 12 in the RΓ direction near R, and from the second valence band to band 14 from a region RΓM plane, where the bands are parallel. The last peak at 16.80 eV is mainly due to transitions from the second valence band to band 16 in the XM direction. At still higher energy the spectrum is without structures and decays very rapidly with photon energy.

3.4. Pressure dependence of band gaps

When the material of interest is compressed, the positions of all critical points cited above are shifted towards an increased energy as compared to that at normal pressure. The LDA does not accurately describe the eigenvalues of the electronic states, which causes quantitative underestimation of the band gaps. These quantities are not well predicted by LDA. However the pressure derivatives of conduction band

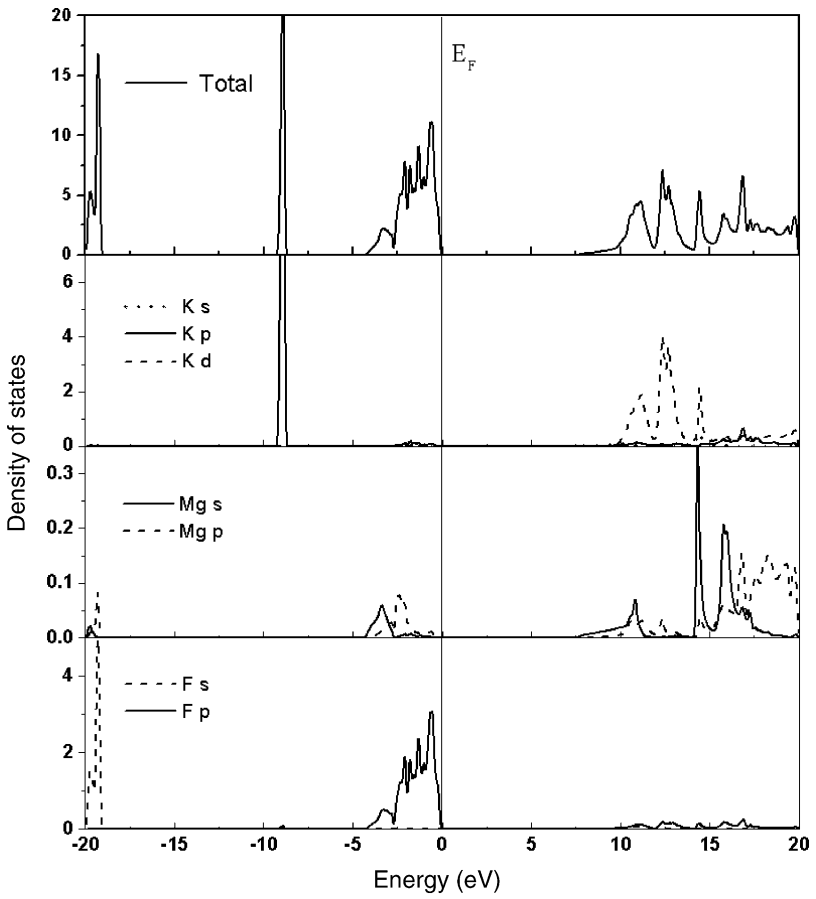

Fig. 4. The calculated total and projected density of states (DOS) for $KMgF_3$.

states [44] and the relative positions are predicted reasonably well by the LDA. The underestimation of the pressure coefficients can probably be attributed to LDA, but for a small percentage compared to the absolute band gaps. We therefore assume that the band gap states calculated within the LDA show the qualitatively correct ordering and dependence on the cell volume. In order to investigate the dependence of the cell volume up on the size of the energy gaps related to conduction band minimum for $KMgF_3$: the band energies at selected symmetry points were examined as a function of cell volume. The results of these calculations for the direct band gaps of this material versus volume are shown in Fig. 6, where the solid lines are linear and quadratic least square fits.

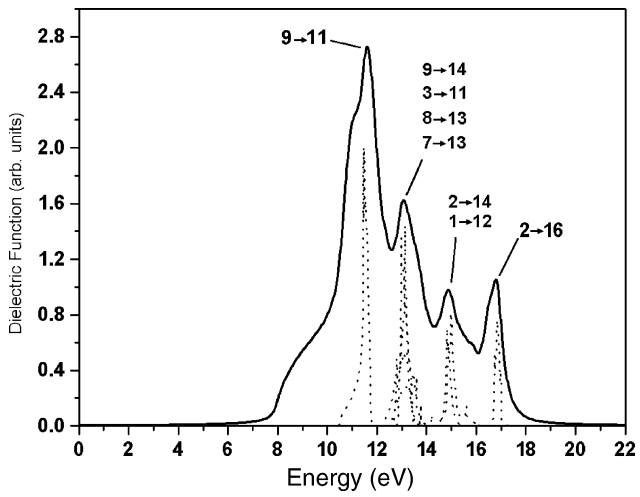

Fig. 5. The imaginary part of the dielectric function for $KMgF_3$ including a life-time broadening of 0.15 eV. The most important interband contributions to the imaginary part of the dielectric function are included.

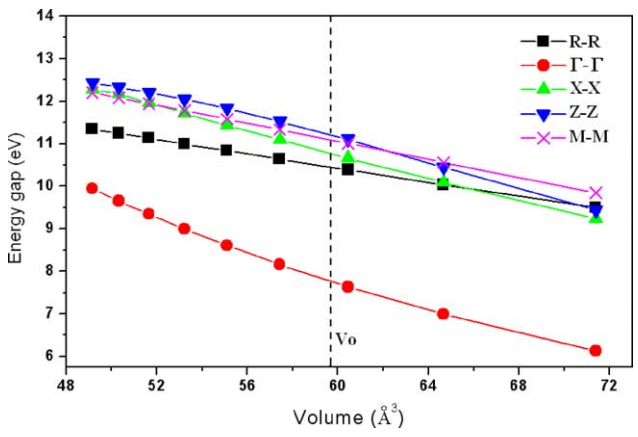

Fig. 6. Calculated dependence of the direct band gaps of $KMgF_3$ on the change of the volume.

Table 2
Calculated linear and quadratic pressure coefficients of important band gaps for $KMgF_3$

	R–R	Γ–Γ	X–X	Z–Z	M–M
$E_i(0)$	10.38	7.68	10.68	11.07	11.00
b	0.06	0.12	0.10	0.11	0.08
c	−0.0014	−0.0014	−0.0017	−0.0023	−0.0014

$E_i(p) = E_i(0) + bp + cp^2$, $b = \partial E_i/\partial p$ in eV GPa^{-1}, $c = \partial^2 E_i/\partial p^2$ in eV GPa^{-2}.

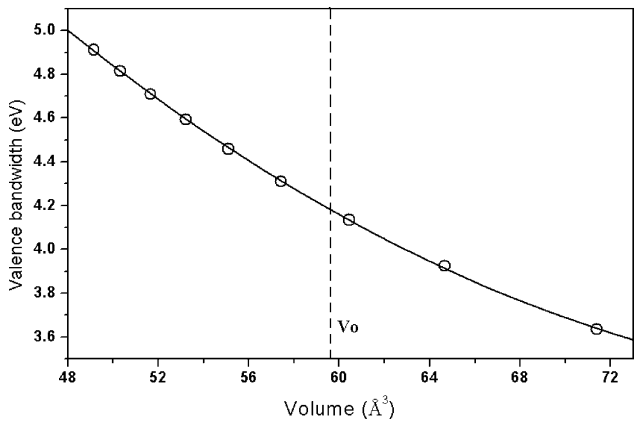

Fig. 7. Calculated dependence of the valence bandwidth of $KMgF_3$ on the change of the volume.

Whereas Table 2 contains the values of linear and quadratic pressure coefficients calculated for the important band gaps in $KMgF_3$. Considering Fig. 6, all energy gaps shown increase with decreasing volume corresponding to an increase of hydrostatic pressure up to 30 GPa. It should be noted that also the minimum of the first valence band at R-point is shifted downwards when volume decreases. This leads to an increase of the valence bandwidth (VBW). Our results showed that the latter increases from 3.6 to 5 eV when going from 71.7 to 48.2 Å^3 for the volume. In Fig. 7 we show the dependence of the VBW on volume variation. Accordingly, the VBW increases monotonically with decreasing volume. Part of this effect arises from hybridization accompanying the change in bonding in $KMgF_3$. Consequently, this reflects the decrease of the ionicity character of $KMgF_3$ under pressure.

4. Summary

We have used the FP-LAPW method to study the structural, electronic and optical properties of the perovskite $KMgF_3$. A detailed investigation of its structural, electronic band structure and different band contributions from the partial and total density of states curves have been made. Our results show that the fundamental band gap of $KMgF_3$ is indirect between Γ and R symmetry points of the Brillouin zone. From the imaginary part of the dielectric function and the real part of the optical conductivity curves we have studied the different optical transitions, for which we have presented the different peak structures associated with their assignment of the interband transitions. The high hydrostatic pressure dependence of the electronic properties of perovskite $KMgF_3$ has been investigated for pressures up 30 GPa using the FP-LAPW. The dependence of the electronic structure on hydrostatic pressure shows a linear behavior.

Acknowledgements

This work was supported by the Swiss National Science Foundation OFES and by the Swiss Federal Office of Education on Science trough COST Action D26.

References

[1] M. Sasago, Oyo Buturi 68 (1999) 520 (in Japanese).
[2] G. Horsch, H. Paus, J. Opt. Commun. 60 (1986) 69.
[3] S. Sugano, R.G. Shulman, Phys. Rev. 130 (1963) 517.
[4] B. Kleinman, M. Karplus, Phys. Rev. B 3 (1971) 24.
[5] T.F. Soules, J.W. Richardson, D.M. Vaught, Phys. Rev. B 3 (1971) 2186.
[6] T.F. Soules, E.J. Kelly, D.M. Vaught, J.W. Richardson, Phys. Rev. B 6 (1972) 1519.
[7] L.F. Mattheiss, Phys. Rev. B 6 (1972) 4718.
[8] R.G. Shulman, Y. Yafet, P. Eisenberger, W.E. Blumberg, Proc. Natl. Acad. Sci. U.S.A. 73 (1976) 1384.
[9] K. Shimamura, H. Sato, A. Bensalah, H. Machida, N. Sarukura, T. Fukuda, in: S.K. Gupta, S.K. Halder, G. Bhagavannarayana (Eds.), Proceedings of the International Workshop on Prep. and Charact. Tech. Imp. Single Crystals, National Physical Laboratory, New Delhi, 2001.
[10] Massa, Babel, 1988 in Victor Luana, Aurora Costales and Angel Martin Pendas, 1996. victor@carbono.quimica.uniovi.es.
[11] A. Darabont, C. Neamtu, S.I. Farcas, Gh. Borodi, J. Cryst. Growth 169 (1996) 89.
[13] H. Remy, F. Hansen, Z. Anorg, Allg. Chem. 283 (1956) 277.
[15] V.W. Goldschmidt, J. Math. Naturvid. Klass 2 (1926) 97.
[16] M. Rousseau, Ph.D. Thesis, Université Paris 6, 1977.
[17] L.M. Reshchikova, Soviet Phys.-Solid State 10 (1969) 2019;
L.M. Reshchikova, Ultrasonics 7 (1969) 212;
L.M. Reshchikova, Fizika Tverdogo Tela (Sankt-Peterburg) 10 (1968) 2558.
[18] H.M. Rosenberg, J.K. Wigmore, Phys. Lett. A 24 (1967) 317.
[19] B. Lal, S.K. Khosa, R. Tickoo, K.K. Bamzai, P.N. Kotru, Mater. Chem. Phys. 83 (2004) 158.
[20] K. Rittenmyer, A.S. Bhalla, L.E. Cross, Mater. Lett. 7 (1989) 380.
[21] Ichiro Nakagawa, Spectrochim. Acta A: Mol. Bio. Spectr. 29 (1973) 1451.
[22] J.P. Perdew, Y. Wang, Phys. Rev. B 45 (1992) 13244.
[23] P. Blaha, K. Schwarz, J. Luits, Wien97, Vienna University of Technology, 1997 (improved and Updated Unix Version of the original copyrighted WIEN-code, which was published in: P. Blaha, K. Schwarz, P. Sorantin, S.B. Trickey, Comput. Phys. Commun. 59 (1990) 399).
[24] P. Blaha, K. Schwarz, J. Luitz, Wien97-Code, in: K. Schwarz (Ed.), TU Wien, ISBN 3-9501031-0-4, 1999.
[25] Blaha, K. Schwarz, W. Faber, J. Luitz, Hyp. Interact. 126 (2000) 389.
[26] H.J. Monkhorst, J.D. Pack, Phys. Rev. B 13 (1976) 5188.
[27] F.D. Murnaghan, Proc. Natl. Acad. Sci. U.S.A. 30 (1944) 244.
[28] M.J. Mehl, Phys. Rev. B 47 (1993) 2493.
[29] L.F. Mattheiss, Phys. Rev. B 2 (1970) 3918.
[30] L.F. Mattheiss, Phys. Rev. 181 (1969) 987.

[31] A.H. Khan, A.J. Leyendecker, Phys. Rev. 135 (1964) 1321.
[32] R.R. Daniels, G. Margaritondo, R.A. Heaton, C.C. Lin, Phys. Rev. B 27 (1983) 3878.
[33] J.H. Beaumont, A.J. Bourdillon, J. Bordas, J. Phys. C 10 (1977) 333.
[34] T. Nishimatsu, T. Takeshi, M. Noriaki, K. Hiroshi, P.A. Yoshiyuki, S. Dorota, F. Kiyoshi, Tsuguo, Jpn. J. Appl. Phys. 41 (2002) 365.
[35] H. Takahashi, R. Onaka, J. Phys. Soc. Jpn. 43 (1977) 2021.
[36] R.A. Heaton, C.C. Lin, Phys. Rev. B 25 (1982) 3538–3549.
[37] R.O. Jones, O. Gunnarsson, Rev. Mod. Phys. 61 (1989) 689.
[38] J.S. Tell, Phys. Rev. 104 (1956) 1760.
[39] L.D. Landau, E.M. Lifshitz, Electrodynamics in Continuous Media, Pergamon Press, Oxford, 1960.
[40] H.A. Kramers, Collected Science Papers, North Holland, Amsterdam, 1956, p. 333.
[41] R.De.L. Kronïg, J. Opt. Soc. Am. 12 (1926) 547.
[42] F. Bassani, G. Pastroi, Parravicini, Electronic States and Optical Transitions in Solids, Pergamon Press, Oxford, 1973.
[44] P. Puschnig, C. Ambrosch-Draxl, Phys. Rev. B 66 (2002) 165105.
[45] C. Ambrosch-Draxl, R. Abt, The Calculation of Optical Properties Within WIEN97, ICTP Lecture Notes 1998, unpublished;
S. Sharma, C. Ambrosch-Draxl, M.A. Khan, P. Blaha, S. Auluck, Phys. Rev. B 60 (1999) 8610.